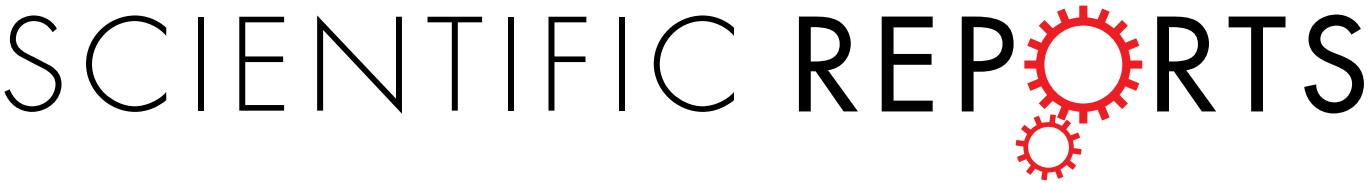

OPEN

Magnetic Resonance Imaging of Phosphocreatine and Determination of BOLD Kinetics in Lower Extremity Muscles using a Dual-Frequency Coil Array

Received: 09 June 2016
Accepted: 01 July 2016
Published: 28 July 2016

Ryan Brown[1,2,3], Oleksandr Khegai[1] & Prodromos Parasoglou[1,2]

Magnetic resonance imaging (MRI) provides the unique ability to study metabolic and microvasculature functions in skeletal muscle using phosphorus and proton measurements. However, the low sensitivity of these techniques can make it difficult to capture dynamic muscle activity due to the temporal resolution required for kinetic measurements during and after exercise tasks. Here, we report the design of a dual-nuclei coil array that enables proton and phosphorus MRI of the human lower extremities with high spatial and temporal resolution. We developed an array with whole-volume coverage of the calf and a phosphorus signal-to-noise ratio of more than double that of a birdcage coil in the gastrocnemius muscles. This enabled the local assessment of phosphocreatine recovery kinetics following a plantar flexion exercise using an efficient sampling scheme with a 6 s temporal resolution. The integrated proton array demonstrated image quality approximately equal to that of a clinical state-of-the-art knee coil, which enabled fat quantification and dynamic blood oxygen level-dependent measurements that reflect microvasculature function. The developed array and time-efficient pulse sequences were combined to create a localized assessment of calf metabolism using phosphorus measurements and vasculature function using proton measurements, which could provide new insights into muscle function.

In vivo phosphorus magnetic resonance spectroscopy (^{31}P-MRS) has been used extensively to assess energy metabolism in many diseases that affect skeletal muscle[1]. ^{31}P-MRS can measure phosphocreatine (PCr) and inorganic phosphate (Pi) kinetics and yield valuable information about muscle mitochondrial function during exercise[2–4].

Due to the low concentration of phosphorus-containing metabolites in human tissue[5] and the low intrinsic sensitivity of ^{31}P-MR, most ^{31}P-MRS studies are performed using small surface coils that are placed adjacent to the muscle of interest[4]. Such coils can provide an adequate signal-to-noise ratio (SNR) in a local region, but they exhibit an inhomogeneous magnetic field and limited coverage. These characteristics typically require lengthy power-demanding adiabatic pulses to generate an excitation field with adequate uniformity and prohibit simultaneous analysis of metabolic activity in multiple lower extremity muscles[6–8]. Meanwhile, birdcage coils have been used to acquire whole-volume ^{31}P-MR data with a homogeneous field distribution but with a reduced SNR compared to surface coils, which can result in compromised spatial-temporal resolution and/or acquisition time[9,10].

^{31}P-MR exercise protocols require suitable temporal resolution to adequately capture mitochondrial function. Previously, we demonstrated a protocol with a birdcage coil at 3 Tesla that provided volumetric measurements of the lower leg with a 24 s temporal resolution[11]. This resolution was reduced to 12 s by combining the SNR advantage at 7 Tesla with an efficient compressed sensing data acquisition scheme[12]. However, this rate can make

[1]Bernard and Irene Schwartz Center for Biomedical Imaging, Department of Radiology, New York University School of Medicine, New York, NY, USA. [2]Center for Advanced Imaging Innovation and Research (CAI2R), Department of Radiology, New York University School of Medicine, New York, NY, USA. [3]NYU WIRELESS, Polytechnic Institute of New York University, 2 Metro Tech Center, Brooklyn, NY, 11201, USA. Correspondence and requests for materials should be addressed to R.B. (email: ryan.brown@nyumc.org)

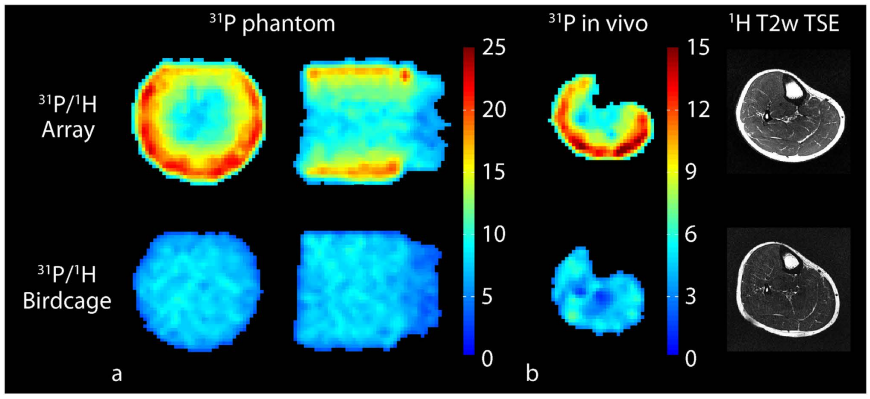

Figure 1. Characterization of the eight-channel ^{31}P module of the developed array. The array provided a similar ^{31}P SNR in the center and greater than 2-fold gain in the periphery over the birdcage in the 42 mM Pi phantom (**a**). Similar results were observed *in vivo* (**b**). The measurements are summarized in Table 1.

Measurement	^{31}P SNR						^{31}P B_1^+ (nT/V)
ROI	GN(lat)	GN(med)	Soleus	TA	TP	Phantom (center)	Phantom (transverse cross-section)
^{31}P/^{1}H Array	12.4 ± 2.0	12.1 ± 2.4	8.4 ± 2.2	8.9 ± 1.4	5.6 ± 0.8	8.2	253.4 ± 14.3
^{31}P/^{1}H Birdcage	5.1 ± 0.7	4.9 ± 0.9	3.8 ± 1.3	4.8 ± 1.3	4.2 ± 1.0	8.0	323.2 ± 6.5

Table 1. Summary of ^{31}P SNR and B_1^+ measurements in the developed array and a commercially available dual-nuclei birdcage. *GN = gastrocnemius, TA = tibialis anterior, TP = tibialis posterior, lat = lateral, med = medial. Values are reported as the mean ± standard deviation within the ROI.

it challenging to accurately model PCr recovery following exercise[13], and it is significantly slower than the rate achieved in studies performed with surface coils and unlocalized spectroscopy sequences (typically 6 s)[14].

Recently, phased array coils have been designed to combine the SNR of surface coils with the volumetric coverage of birdcage coils for low SNR, non-proton applications[15–27]. In this study, we developed and evaluated a ^{31}P/^{1}H array for lower extremity MRI. The array consisted of an encompassing eight-channel ^{31}P module to provide volumetric coverage of the lower extremities along with a high SNR that can be exchanged for temporal resolution. Additionally, the developed array was equipped with an integrated eight-channel ^{1}H module that enabled clinical-quality MRI measurements, which is essential for assessing micro- and macro-vascular functions in skeletal muscle using dynamic techniques such as blood oxygenation level dependent (BOLD) MRI[28] and arterial spin labeling (ASL)[29]. We generated benchmark performance measurements to compare the developed array to commercially available alternatives. Preliminary *in vivo* experiments additionally demonstrate the results of volumetric ^{31}P and ^{1}H imaging with high spatial and temporal resolution during lower extremity exercise protocols.

Results

^{31}P benchmark measurements. *In vivo* measurements showed that the SNR provided by the ^{31}P module of the developed eight-channel array was more than 2.4 times greater than the SNR of the commercially available single-channel reference volume coil (birdcage) in peripheral muscles such as the medial and lateral gastrocnemius, which are recruited for pedal flexion (see Fig. 1 and Table 1). The SNR gain in locations near the center of the calf, such as the tibialis posterior, were in the range of 30%. The transmission efficiencies for spin excitation in the central transverse plane of a water phantom (15 cm diameter, 2 L, doped with 42 mM Pi) were 253.4 ± 14.3 and 323.2 ± 6.5 nT/V for the developed array and reference coil, respectively. The ~30% reduction in transmission efficiency compared to the reference coil was partially due to losses in the multi-stage power divider that is required in the interface chain as well as inter-element coupling. Both losses were considered to be tolerable consequences of the multi-element transmission configuration.

^{1}H benchmark measurements. The ^{1}H SNR provided by the developed dual-nuclei array was superior to the dual-nuclei volume coil (approximately 2.4 times greater in the gastrocnemius muscles) and similar to (within 15%) that of a state-of-the-art 15-channel mono-nuclear clinical array. The ^{1}H transmission efficiency and uniformity were similar for all three coils (see Fig. 2 and Table 2). The spin echo anatomical images exhibited good quality with no signs of artifacts.

Dynamic ^{31}P-MRI. Figure 3 shows dynamic imaging of PCr using a spectrally selective ^{31}P-FLORET pulse sequence with a 6-s temporal resolution. The time series SNR of the PCr signal from the gastrocnemius muscle at rest was 19.0. A 30-year-old male participant performed plantar flexions at 0.33 Hz according to an acoustic

Measurement	^{1}H SNR					^{1}H B1+ (nT/V)
ROI	GN(lat)	GN(med)	Soleus	TA	TP	Calf (transverse cross section)
^{31}P/^{1}H Array	2.41 ± 0.23	2.52 ± 0.38	1.82 ± 0.24	1.30 ± 0.14	1.28 ± 0.13	89.1 ± 8.8
^{31}P/^{1}H Birdcage	1.08 ± 0.14	0.97 ± 0.08	1.14 ± 0.10	0.93 ± 0.11	1.26 ± 0.11	98.7 ± 8.4
Clinical ^{1}H Array	2.47 ± 0.23	2.16 ± 0.28	1.97 ± 0.34	1.45 ± 0.17	1.50 ± 0.16	87.4 ± 6.1

Table 2. Summary of ^{1}H SNR and B_1^+ measurements in the developed array and two commercially available coils. *GN = gastrocnemius, TA = tibialis anterior, TP = tibialis posterior, lat = lateral, med = medial. Values are reported as the mean ± standard deviation within the ROI.

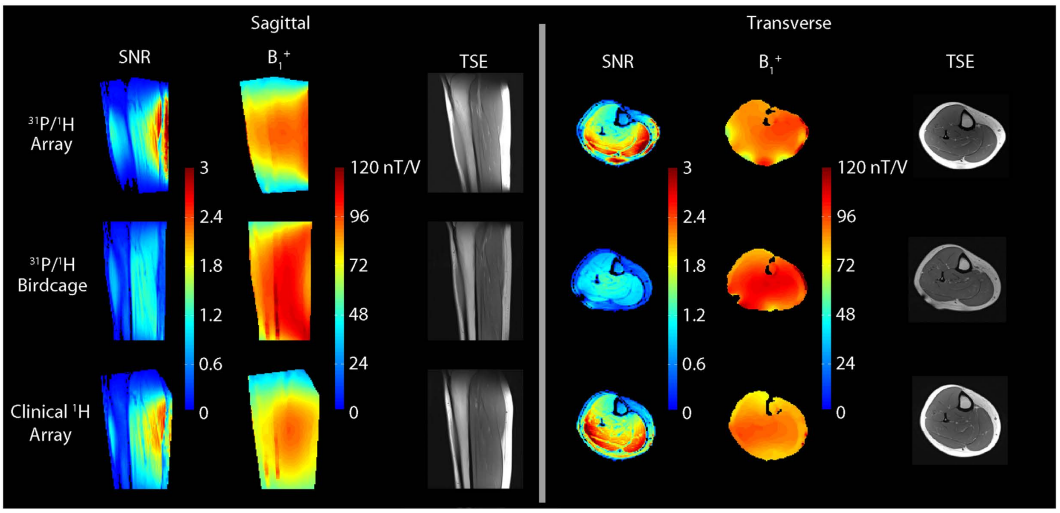

Figure 2. Normalized ^{1}H SNR maps (first and fourth columns), B_1^+ maps (second and fifth columns), and TSE images (third and last columns) acquired with the eight-channel ^{1}H module (top row) of the developed array. The array showed favorable performance over the dual-frequency birdcage coil (middle) and similar performance to the clinical 15-channel ^{1}H array (bottom). The measurements are summarized in Table 2.

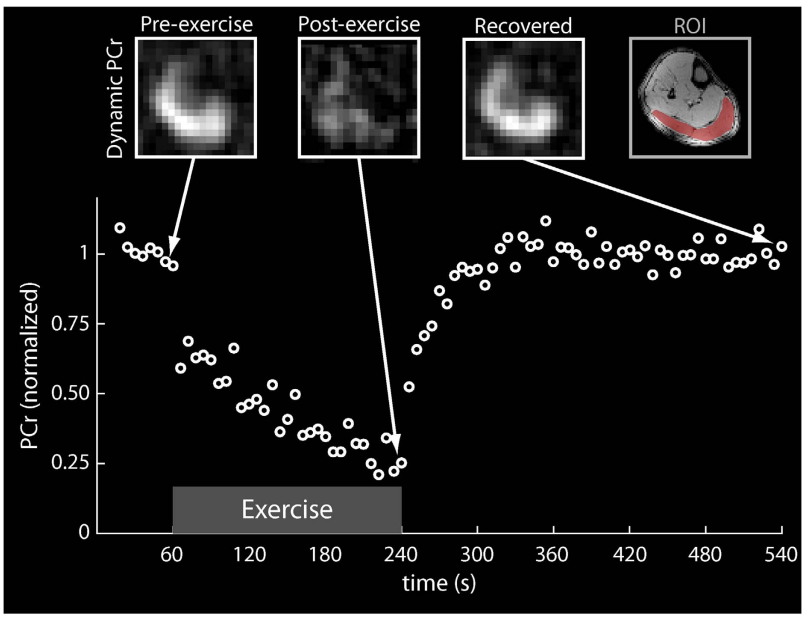

Figure 3. Dynamic ^{31}P PCr (top row) images acquired using the developed coil array in the calf muscle at different time points during the plantar flexion exercise protocol with the PCr signal time course (bottom) from the segmented gastrocnemius muscle (top right).

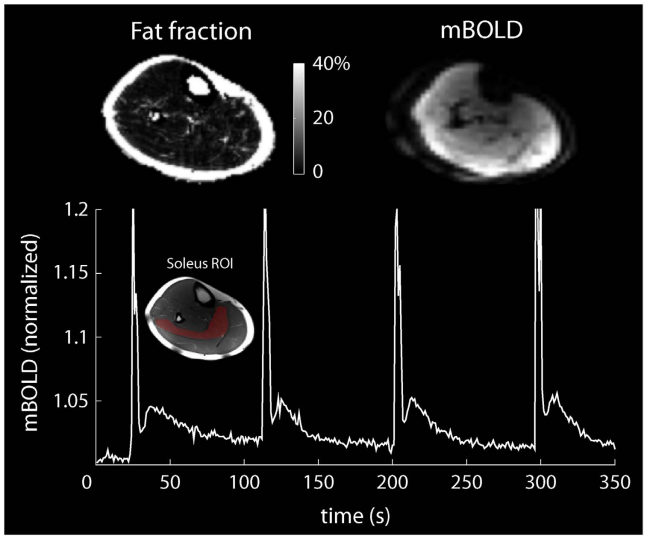

Figure 4. ***In vivo*** **fat fraction and mBOLD images (top row) and mBOLD signal evolution in the soleus muscle (bottom row, ROI inset) following maximum voluntary isometric plantar flexions.**

cue using an MR compatible ergometer that was built in-house[30]. The PCr signal in the gastrocnemius muscle was fit to a single exponential recovery function to determine PCr depletion (77%) and the PCr resynthesis rate ($k_{PCr} = 20.5$ s, $r^2 = 0.91$).

^{1}H-MRI. Many diseases that are known to affect skeletal muscle metabolism, such as obesity, diabetes, and muscular dystrophy, also result in fat infiltration into the muscle[31]. To demonstrate the ^{1}H-MRI capability of the coil, we calculated water and fat fraction maps using the Hierarchical IDEAL method[32] from data acquired with a multi-echo three-dimensional gradient echo sequence in a 31-year-old male volunteer with a BMI of 25.5 (see Fig. 4). Low fat infiltration (<2.5%) was observed in all muscle groups of the lower leg in this subject.

BOLD changes in the soleus muscle were measured following voluntary maximal isometric plantar flexion contractions using a one-shot gradient-recalled echo-planar sequence. We acquired images during a 10 min period while the subject performed 1-s isometric contractions every 90 s. The spikes in the BOLD signal during the contractions were followed by delayed transient signal increases (see Fig. 4). The relative BOLD signal increase (ΔS_{max}) was 2.9%, while the time-to-peak (TTP) was 12.5 s.

Discussion

In this study, we demonstrated that an eight-channel ^{31}P transmit/receive RF array paired with a "nested" eight-channel ^{1}H array could provide high-quality ^{31}P and clinical-quality ^{1}H data on a clinical 3 Tesla MR device. We combined the coil with efficient pulse sequences, (i.e., ^{31}P-FLORET) to measure PCr kinetics following exercise with a 6-s temporal resolution. To the best of our knowledge, this temporal resolution is the highest achieved with a volumetric imaging pulse sequence, and it is comparable to the resolution obtained using unlocalized spectroscopy[11,12,33].

The essential goal of this project was to develop a coil that facilitates acquisition of high-quality ^{31}P and ^{1}H MR data without the need to reposition the subject, which is required when two separate mono-nuclear coils are used. Our array provided a substantial ^{31}P SNR gain over a conventional birdcage coil. The ^{31}P structure was free of the SNR-lowering circuitry that may be found in dual-nuclei coils, such as trap circuits or in-line positive-intrinsic-negative (PIN) diodes[34,35]. The proposed approach resulted in ^{31}P SNR gains of 1.3- to 2.4-fold *in vivo*. By combining the ^{31}P transmit and receive functionalities into a single structure, a separate transmit coil was eliminated as well as the lossy components, such as fuses and detuning circuits, that are required in receive-only coils. In transmit mode, we drove the structure with circular polarization to generate an excitation field with a uniformity similar to that of the reference birdcage, which may eliminate the need for adiabatic excitation pulses that can be very lengthy, particularly when inverting deep lying spins. Our array additionally provided ^{1}H imaging and B_0 shimming capabilities with performance that was similar to that of a clinical device. This development enabled us to create comprehensive multinuclear MR protocols that can minimize experimental variability by avoiding subject repositioning, which reduces scan time[36], as well as enable interleaved or simultaneous multinuclear acquisition using specialized pulse sequences and back-end RF hardware[33,37,38].

In summary, our ^{31}P/^{1}H array offers a unique ability to investigate several aspects of muscle function, including regional perfusion[39], blood tissue oxygenation through ^{1}H-MR[28,40], and intracellular pH and mitochondrial function[4] through ^{31}P-MR, in healthy and disease states. Relatively high spatial/temporal resolution multi-nuclear MR can be performed over the entire calf with the developed array and time-efficient pulse sequences, which can potentially provide new insights into vasculature function and metabolic activity in muscles.

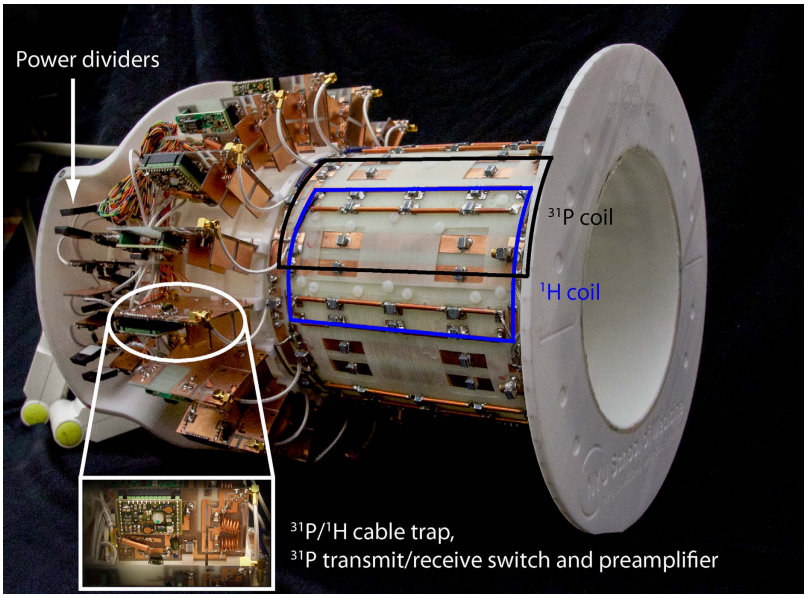

Figure 5. Photograph of the developed ^{31}P/^{1}H array with the protective cover removed. Overlays highlight an interface board that accommodates the cable trap, transmit/receive switch, and the preamplifier for each coil as well as the power dividers, a ^{31}P coil (black), and an ^{1}H coil (blue).

Methods

^{31}P/^{1}H coil design. The main objective of this project was to construct a ^{31}P/^{1}H lower extremity coil with a high ^{31}P SNR to facilitate dynamic imaging of phosphocreatine kinetics on a 3 Tesla MRI scanner. The secondary objectives included obtaining a uniform ^{31}P transmit magnetic field (B_1^+) and developing a ^{1}H module for anatomical localization, dynamic imaging (i.e. BOLD), and B_0 shimming. Two (^{31}P and ^{1}H) transmit/receive arrays were constructed to accomplish these objectives. Both arrays were made up of eight loop coils that encircled the 17-cm-diameter housing structure. The ^{1}H array was offset in the azimuthal direction by 22.5° (see Figs 5 and 6) to reduce shielding caused by the ^{31}P array. All coils were tuned to 49.9 MHz (^{31}P) or 123.2 MHz (^{1}H) and matched to 50 Ω while loaded with a water-based gel phantom[41] with dielectric properties that were designed to mimic muscle tissue[42]. Neighboring and next-nearest coils were decoupled via geometric overlap[43] and lumped element inductors, respectively.

To generate circularly polarized B_1^+ fields, we drove the ^{31}P and ^{1}H arrays using separate eight-way power splitters that each consisted of three stages of Wilkinson power dividers and quadrature hybrids arranged to provide outputs with 45° phase offsets that corresponded to the azimuthal position of the coils. Individual power splitter outputs were connected to transmit/receive switches to protect the preamplifiers during transmission. The transmit/receive switches utilized a quarter-wavelength-based design similar to a previously outlined method[44]. Individual cable traps were connected to each coil port, and the cable traps were tuned to block common mode current on the coaxial cable shield at ^{31}P and ^{1}H resonant frequencies. Preamplifier decoupling was accomplished by installing lumped-element phase-shifters at the preamplifier input such that its low input impedance was translated into an inductance that formed a parallel resonant circuit with the coil match capacitor[43].

Coil benchmarking. All imaging experiments were performed on a 3 Tesla MRI scanner (Prisma, Siemens Medical Solutions, Erlangen, Germany). The study was fully compliant with the Health Insurance Portability and Accountability Act, and the New York University Institutional Review Board approved the protocol. We scanned human subjects after obtaining their informed written consent. The methods were conducted in accordance with Food and Drug Administration guidelines. We restricted transmit power to 10 W/kg based on MR thermometry measurements using a procedure similar to the method described in ref. 45 to enforce a two-fold safety buffer below the 20 W/kg limit set by the International Electrotechnical Commission (IEC document 60601-2-33 2010).

We performed SNR and B_1^+ benchmark measurements with the developed array as well as two commercial coils available at our Center including 1) a dual-nuclei ^{31}P/^{1}H birdcage knee coil (~19 cm in diameter, Rapid Biomedical, Rimpar, Germany) and 2) a state-of-the-art clinical single-nuclei ^{1}H 15-channel knee array (~18 cm in diameter, "TxRx 15Ch Knee Coil", Quality Electrodynamics, Mayfield, OH, USA). Raw SNR maps were calculated from the signal and noise (with the RF pulse amplitude set to zero) measurements acquired with a gradient echo pulse sequence and processed with the optimal array combination method[43,46]. The ^{31}P/^{1}H imaging parameters were as follows: TR = 10/3.5 s, TE = 6.4/3.6 ms, flip angle = 76/10°, voxel size = 7.8 × 7.8 × 50.0/2.0 × 2.0 × 5.0 mm^3, and acquisition time = 642/338 s. To account for the spatially dependent ^{1}H B_1^+, the ^{1}H raw SNR maps were scaled according to $SNR = SNR_{raw}\frac{(1-\cos\alpha)e^{-TR/T_1}}{(1-e^{-TR/T_1})\sin\alpha}$, where α is the flip angle, TR is the repetition time, and $T_1 = 1.4$ s is the relaxation time of the muscle[47]. We calculated the SNR in various muscles by manually segmenting co-registered spin echo anatomical images in the central transverse plane of the coils.

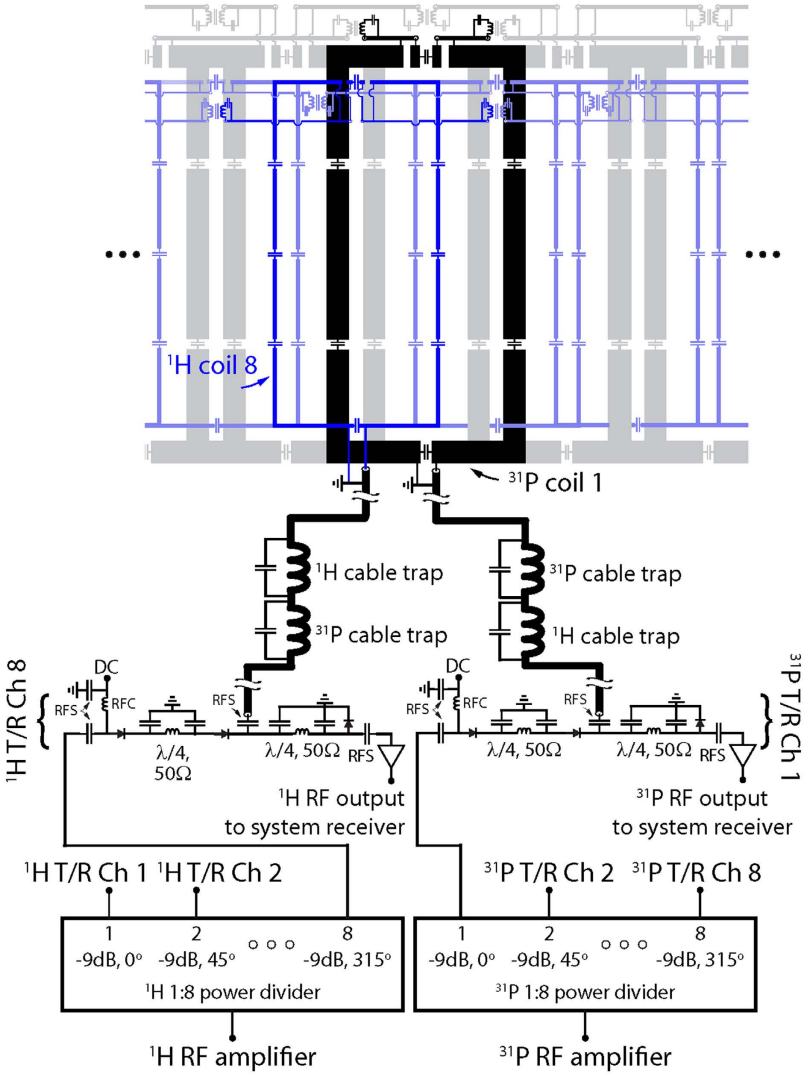

Figure 6. Unrolled schematic diagram of the ^{31}P/^{1}H coil array and interface. For simplicity, single ^{31}P (black) and ^{1}H (blue) coils of the 16-channel nested array are highlighted whereas neighboring elements are displayed in a semi-transparent fashion. Abbreviations: RFC = radio frequency choke and RFS = radio frequency short.

The ^{1}H B_1^+ field was measured using the method described in ref. 48. Because the pulse sequence was not available for non-proton nuclei, we performed ^{31}P B_1^+ mapping by scaling the period of a sine curve fit to the pixel-wise signal intensities of a series of gradient echo images that were collected with a range of imaging pulse amplitudes. For both nuclei, the B_1^+ mapping resolution was matched to the resolution of the respective SNR measurements.

Dynamic ^{31}P/^{1}H-MR experiments. We acquired dynamic ^{31}P data using a three-dimensional non-Cartesian fermat looped, orthogonally encoded trajectories (FLORET) sequence[49,50] with a narrowband Gaussian-shaped pulse (duration: 12 ms; bandwidth: 125 Hz) to excite a single metabolite of the ^{31}P spectrum (i.e., PCr). The participant performed 180 s plantar flexion exercises at 0.33 Hz according to an acoustic cue on an in-house-developed, MR-compatible ergometer[30]. During exercise, the participant moved the footplate of the ergometer through a 30° range of motion. Resistance was applied by rubber tubing and was set to approximately 40% of the subject's maximum voluntary contraction (MVC). Images with 6 s temporal resolution were acquired serially before (baseline), during, and after completing the exercise. The acquisition parameters of the FLORET sequence were as follows: TR = 0.5 s, FA = 25°, 3 hubs at 45°, 4 interleaves per hub, 1.7 cm nominal isotropic resolution, 6 s acquisition time per image, and 9 min total acquisition time. The plot in Fig. 3 shows a signal from the gastrocnemius muscle that was manually segmented in a co-registered ^{1}H spin echo image.

To measure fat content in the muscle, we applied an ^{1}H three-dimensional gradient echo sequence with the following parameters: TE = 2.1, 2.8 and 3.7 ms, flip angle = 3°; TR = 12 ms, FOV = 22 × 22 × 20 cm^3, acquisition matrix = 128 × 128 × 40, and total acquisition time = 3 min. Water and fat fraction maps were calculated using the Hierarchical IDEAL method[32].

BOLD dynamics following maximal isometric contractions were measured using an ^{1}H one-shot gradient-recalled echo-planar sequence with the following parameters: TR = 1 s, TE = 35 ms, FOV = 25 × 25 cm^2, slice thickness = 1 cm, acquisition matrix = 64 × 64, and acquisition time = 10 min. We measured the post-contractile response in the soleus muscle, which was characterized by the peak ΔS_{max} and the TTP[51]. The plot in Fig. 4 shows the signal from the soleus muscle that was manually segmented in a co-registered ^{1}H spin echo image.

References

1. Kemp, G., Ahmad, R., Nicolay, K. & Prompers, J. Quantification of skeletal muscle mitochondrial function by 31P magnetic resonance spectroscopy techniques: a quantitative review. *Acta Physiologica* **213,** 107–144 (2015).
2. Arnold, D. L., Matthews, P. M. & Radda, G. K. Metabolic recovery after exercise and the assessment of mitochondrial function *in vivo* in human skeletal-muscle by means of 31P NMR. *Magnetic Resonance in Medicine* **1,** 307–315, doi: 10.1002/mrm.1910010303 (1984).
3. Kemp, G. J., Taylor, D. J. & Radda, G. K. Control of phosphocreatine resynthesis during recovery from exercise in human skeletal-muscle. *Nmr in Biomedicine* **6,** 66–72, doi: 10.1002/nbm.1940060111 (1993).
4. Prompers, J. J. *et al.* Dynamic MRS and MRI of skeletal muscle function and biomechanics. *NMR in Biomedicine* **19,** 927–953, doi: 10.1002/nbm.1095 (2006).
5. Kemp, G. J., Meyerspeer, M. & Moser, E. Absolute quantification of phosphorus metabolite concentrations in human muscle *in vivo* by P-31 MRS: a quantitative review. *Nmr in Biomedicine* **20,** 555–565, doi: 10.1002/nbm.1192 (2007).
6. Fiedler, G. B. *et al.* Localized semi-LASER dynamic 31P magnetic resonance spectroscopy of the soleus during and following exercise at 7 T. *MAGMA* **28,** 493–501 (2015).
7. Befroy, D. E., Rothman, D. L., Petersen, K. F. & Shulman, G. I. 31P-magnetization transfer magnetic resonance spectroscopy measurements of *in vivo* metabolism. *Diabetes* **61,** 2669–2678 (2012).
8. Choi, S. *et al.* 31P Magnetic Resonance Spectroscopy Assessment of Muscle Bioenergetics as a Predictor of Gait Speed in the Baltimore Longitudinal Study of Aging. *The journals of gerontology. Series A, Biological sciences and medical sciences*, doi: 10.1093/gerona/glw059 (2016).
9. Greenman, R. L. Quantification of the P-31 metabolite concentration in human skeletal muscle from RARE image intensity. *Magnetic Resonance in Medicine* **52,** 1036–1042, doi: 10.1002/mrm.20258 (2004).
10. Parasoglou, P., Xia, D., Chang, G. & Regatte, R. R. 3D-Mapping of Phosphocreatine Concentration in the Human Calf Muscle at 7 T: Comparison to 3 T. *Magnetic Resonance in Medicine* **70,** 1616–1625 (2013).
11. Parasoglou, P., Xia, D., Chang, G. & Regatte, R. R. Dynamic three-dimensional imaging of phosphocreatine recovery kinetics in the human lower leg muscles at 3 T and 7 T: a preliminary study. *NMR Biomed* **26,** 348–356, doi: 10.1002/nbm.2866 (2013).
12. Parasoglou, P., Feng, L., Xia, D., Otazo, R. & Regatte, R. R. Rapid 3D-Imaging of Phosphocreatine Recovery Kinetics in the Human Lower Leg Muscles with Compressed Sensing. *Magnetic Resonance in Medicine* **68,** 1738–1746 (2012).
13. Arsac, L. M., Thiaudiere, E., Diolez, P. & Gerville-Reache, L. Parameter estimation in modeling phosphocreatine recovery in human skeletal muscle. *European Journal of Applied Physiology* **91,** 419–424, doi: 10.1007/s00421-003-1001-5 (2004).
14. Edwards, L. M. *et al.* Integrating muscle cell biochemistry and whole-body physiology in humans: 31P-MRS data from the InSight trial. *Sci Rep* **3** (2013).
15. Goluch, S. *et al.* A form-fitted three channel 31P, two channel 1H transceiver coil array for calf muscle studies at 7 T. *Magnetic Resonance in Medicine* **73,** 2376–2389 (2015).
16. Avdievich, N. I. & Hetherington, H. P. 4 T Actively detuneable double-tuned 1H/31P head volume coil and four-channel 31P phased array for human brain spectroscopy. *J Magn Reson* **186,** 341–346, doi: 10.1016/j.jmr.2007.03.001 (2007).
17. van der Velden, T. A. *et al.* Radiofrequency configuration to facilitate bilateral breast 31P MR spectroscopic imaging and high-resolution MRI at 7 Tesla. *Magn Reson Med*, doi: 10.1002/mrm.25573 (2014).
18. Mirkes, C. *et al.* ^{31}P CSI of the human brain in healthy subjects and tumor patients at 9.4 T with a three-layered multi-nuclear coil: initial results. *Magma,* doi: 10.1007/s10334-016-0524-9 (2016).
19. Brown, R., Lakshmanan, K., Madelin, G. & Parasoglou, P. A nested phosphorus and proton coil array for brain magnetic resonance imaging and spectroscopy. *Neuroimage* **124,** 602–611, doi: 10.1016/j.neuroimage.2015.08.066 (2016).
20. Hardy, C. J., Bottomley, P. A., Rohling, K. W. & Roemer, P. B. An NMR phased array for human cardiac 31P spectroscopy. *Magn Reson Med* **28,** 54–64 (1992).
21. Panda, A. *et al.* Phosphorus liver MRSI at 3 T using a novel dual-tuned eight-channel (3)(1)P/(1)H H coil. *Magn Reson Med* **68,** 1346–1356, doi: 10.1002/mrm.24164 (2012).
22. Webb, A. G. & Smith, N. In *ISMRM* 3818 (Stockholm, Sweden, 2010).
23. Brown, R. *et al.* A flexible nested sodium and proton coil array with wideband matching for knee cartilage MRI at 3 T. *Magn Reson Med*, doi: 10.1002/mrm.26017 (2015).
24. Brown, R. *et al.* Design of a nested eight-channel sodium and four-channel proton coil for 7 T knee imaging. *Magn Reson Med* **70,** 259–268, doi: 10.1002/mrm.24432 (2013).
25. Moon, C. H., Kim, J. H., Zhao, T. & Bae, K. T. Quantitative (23) Na MRI of human knee cartilage using dual-tuned (1) H/(23) Na transceiver array radiofrequency coil at 7 tesla. *J Magn Reson Imaging* **38,** 1063–1072, doi: 10.1002/jmri.24030 (2013).
26. Kaggie, J. D. *et al.* A 3 T sodium and proton composite array breast coil. *Magn Reson Med* **71,** 2231–2242, doi: 10.1002/mrm.24860 (2014).
27. Lakshmanan, K., Brown, R., Madelin, G., Boada, F. E. & Wiggins, G. In *ISMRM* 4879 (Milan, Italy, 2014).
28. Towse, T. F. *et al.* Comparison of muscle BOLD responses to arterial occlusion at 3 and 7 Tesla. *Magnetic Resonance in Medicine* (2015).
29. Englund, E. K. *et al.* Multiparametric Assessment of Vascular Function in Peripheral Artery Disease Dynamic Measurement of Skeletal Muscle Perfusion, Blood-Oxygen-Level Dependent Signal, and Venous Oxygen Saturation. *Circulation: Cardiovascular Imaging* **8,** e002673 (2015).
30. Che, X., Brown, R., Alon, L., Regatte, R. R. & Parasoglou, P. In *ISMRM* 4522 (Singapore, 2016).
31. Hilton, T. N., Tuttle, L. J., Bohnert, K. L., Mueller, M. J. & Sinacore, D. R. Excessive adipose tissue infiltration in skeletal muscle in individuals with obesity, diabetes mellitus, and peripheral neuropathy: association with performance and function. *Physical therapy* **88,** 1336–1344, doi: 10.2522/ptj.20080079 (2008).
32. Tsao, J. & Jiang, Y. Hierarchical IDEAL: Fast, robust, and multiresolution separation of multiple chemical species from multiple echo times. *Magnetic Resonance in Medicine* **70,** 155–150, doi: 10.1002/mrm.24441 (2012).
33. Meyerspeer, M. *et al.* Simultaneous and interleaved acquisition of NMR signals from different nuclei with a clinical MRI scanner. *Magnetic resonance in medicine* (2015).
34. Schnall, M. D., Subramanian, V. H., Leigh, J. S. & Chance, B. A new double-tuned probe for concurrent 1H and 31P NMR. *J Magn Reson* **65,** 122–129 (1985).
35. Ha, S., Hamamura, M. J., Nalcioglu, O. & Muftuler, L. T. A PIN diode controlled dual-tuned MRI RF coil and phased array for multi nuclear imaging. *Phys Med Biol* **55,** 2589–2600, doi: S0031-9155(10)40698-3 [pii] 10.1088/0031-9155/55/9/011 (2010).

36. Wary, C. *et al.* Investigating glycogenosis type III patients with multi-parametric functional NMR imaging and spectroscopy. *Neuromuscular Disord* **20,** 548–558 (2010).
37. Gonen, O. *et al.* Simultaneous and interleaved multinuclear chemical-shift imaging, a method for concurrent, localized spectroscopy. *Journal of Magnetic Resonance, Series B* **104,** 26–33 (1994).
38. Thulborn, K. R., Soffe, N. F. & Radda, G. K. Simultaneous *in vivo* measurement of oxygen utilization and high-energy phosphate metabolism in rabbit skeletal muscle by multinuclear 1 H and 31 P NMR. *Journal of Magnetic Resonance* (*1969*) **45,** 362–366 (1981).
39. Englund, E. K. *et al.* Combined measurement of perfusion, venous oxygen saturation, and skeletal muscle T2* during reactive hyperemia in the leg. *Journal of Cardiovascular Magnetic Resonance* **15,** 70 (2013).
40. Slade, J. M., Towse, T. F., Gossain, V. V. & Meyer, R. A. Peripheral microvascular response to muscle contraction is unaltered by early diabetes but decreases with age. *J Appl Physiol* **111,** 1361–1371 (2011).
41. Duan, Q. *et al.* Characterization of a dielectric phantom for high-field magnetic resonance imaging applications. *Med Phys* **41,** 102303, doi: 10.1118/1.4895823 (2014).
42. Gabriel, S., Lau, R. W. & Gabriel, C. The dielectric properties of biological tissues: III. Parametric models for the dielectric spectrum of tissues. *Phys Med Biol* **41,** 2271–2293 (1996).
43. Roemer, P. B., Edelstein, W. A., Hayes, C. E., Souza, S. P. & Mueller, O. M. The NMR phased array. *Magn. Reson. Med.* **16,** 192–225 (1990).
44. Shajan, G. *et al.* Design and evaluation of an RF front-end for 9.4 T human MRI. *Magn Reson Med* **66,** 596–604, doi: 10.1002/mrm.22808 (2011).
45. Brown, R. *et al.* Design and application of combined 8-channel transmit and 10-channel receive arrays and radiofrequency shimming for 7-T shoulder magnetic resonance imaging. *Invest Radiol* **49,** 35–47, doi: 10.1097/RLI.0b013e3182a5662d (2014).
46. Kellman, P. & McVeigh, E. R. Image reconstruction in SNR units: a general method for SNR measurement. *Magn Reson Med* **54,** 1439–1447, doi: 10.1002/mrm.20713 (2005).
47. Gold, G. E. *et al.* Musculoskeletal MRI at 3.0 T: relaxation times and image contrast. *AJR Am J Roentgenol* **183,** 343–351, doi: 10.2214/ajr.183.2.1830343 (2004).
48. Breton, E., McGorty, K., Wiggins, G. C., Axel, L. & Kim, D. Image-guided radio-frequency gain calibration for high-field MRI. *NMR Biomed* **23,** 368–374, doi: 10.1002/nbm.1471 (2010).
49. Pipe, J. G. *et al.* A new design and rationale for 3D orthogonally oversampled k-space trajectories. *Magn Reson Med* **66,** 1303–1311, doi: 10.1002/mrm.22918 (2011).
50. Madelin, G., Kline, R., Walvick, R. & Regatte, R. R. A method for estimating intracellular sodium concentration and extracellular volume fraction in brain *in vivo* using sodium magnetic resonance imaging. *Sci Rep* **4,** 4763, doi: 10.1038/srep04763 (2014).
51. Meyer, R. A. *et al.* BOLD MRI mapping of transient hyperemia in skeletal muscle after single contractions. *NMR Biomed* **17,** 392–398, doi: 10.1002/nbm.893 (2004).

Acknowledgements

The authors thank Karthik Lakshmanan for insightful discussions on coil design, Guillaume Madelin for the FLORET pulse sequence, Xuejiao Che for assistance with transmit/receive switches, Riccardo Lattanzi for the SNR calculation script, Leeor Alon and Martijn Cloos for MR thermometry tools, and Jerzy Walczyk for construction of the coil housing. This work was partially supported by NIH grant R01DK106292 and was performed under the rubric of the Center for Advanced Imaging Innovation and Research (CAI^{2}R, www.cai2r.net) at the New York University School of Medicine, which is an NIBIB Biomedical Technology Resource Center (NIH P41 EB017183).

Author Contributions

R.B. designed and constructed the coil and prepared Figures 1, 2, 5, and 6. P.P. and O.K. prepared Figures 3 and 4. All authors designed and performed the experiments, analyzed data and contributed to the manuscript text.

Additional Information

Competing financial interests: RB discloses the US patent, "Multi-Nuclei MRI Coil," 13/866,728,2013, which is related to this work. PP and OK declare no financial conflicts of interest.

How to cite this article: Brown, R. *et al.* Magnetic Resonance Imaging of Phosphocreatine and Determination of BOLD Kinetics in Lower Extremity Muscles using a Dual-Frequency Coil Array. *Sci. Rep.* **6**, 30568; doi: 10.1038/srep30568 (2016).